Joule

CellPress

Article

A Multi-functional Molecular Modifier Enabling Efficient Large-Area Perovskite Light-Emitting Diodes

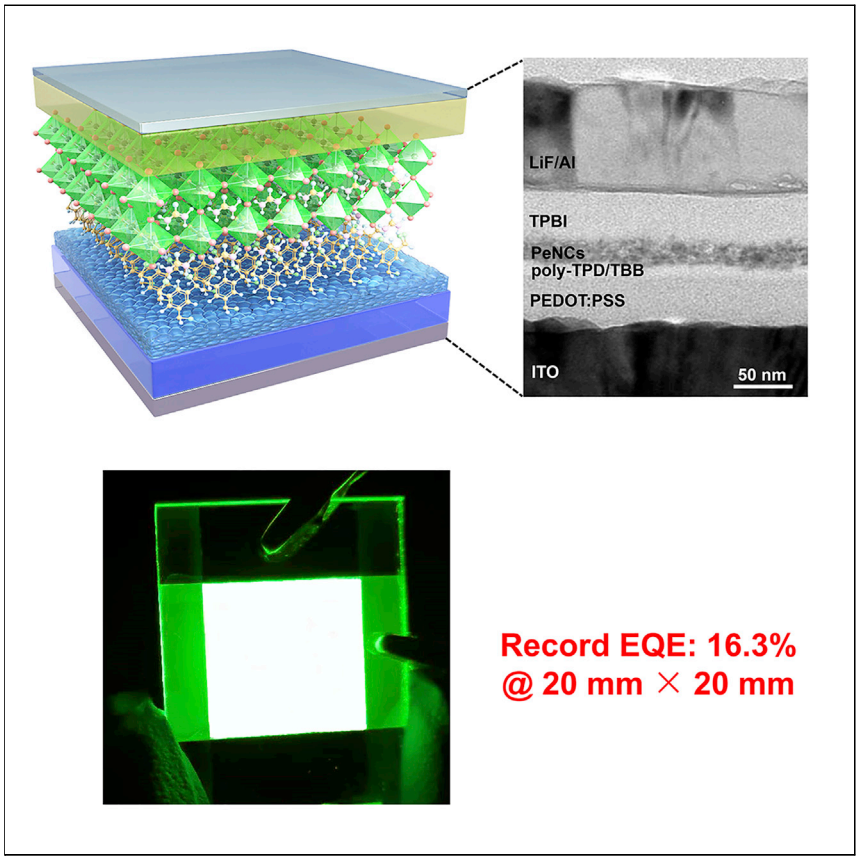

We developed a molecular interface control strategy that eliminates pinholes in perovskites by controlling the dynamics of film formation. The approach simultaneously passivates defects in perovskites by incorporating Br. As a result, the strategy prevents both shorts and non-radiative recombination, all the while providing improved charge injection and balanced charge transport. These improvements enable a 20 mm × 20 mm perovskite LED with an external quantum efficiency of over 16%, the record efficiency for large-area perovskite electroluminescent devices.

Haoran Wang, Xiwen Gong, Dewei Zhao, ..., Yanfa Yan, Edward H. Sargent, Xuyong Yang

yanfa.yan@utoledo.edu (Y.Y.)
ted.sargent@utoronto.ca (E.H.S.)
yangxy@shu.edu.cn (X.Y.)

HIGHLIGHTS

A molecular modification strategy to prepare uniform large-area perovskite films

Significant reduction in shorts and non-radiative recombination in emissive layers

A 20 mm × 20 mm large-area perovskite LED with a record EQE of over 16%

Wang et al., Joule 4, 1977–1987
September 16, 2020
https://doi.org/10.1016/j.joule.2020.07.002

Joule

CellPress

Article

A Multi-functional Molecular Modifier Enabling Efficient Large-Area Perovskite Light-Emitting Diodes

Haoran Wang,[1,6] Xiwen Gong,[2,6] Dewei Zhao,[3,4,6] Yong-Biao Zhao,[2,6] Sheng Wang,[1] Jianfeng Zhang,[1] Lingmei Kong,[1] Bin Wei,[1] Rafael Quintero-Bermudez,[2] Oleksandr Voznyy,[2] Yuequn Shang,[5] Zhijun Ning,[5] Yanfa Yan,[4,*] Edward H. Sargent,[2,*] and Xuyong Yang[1,7,*]

SUMMARY

With rapid progress in perovskite light-emitting diodes (PeLEDs), the electroluminescence performance of large-area is of increasing interest. We investigated why large-area performance lags behind that achieved in laboratory-scale devices and found that defects in perovskite films—emerging from thermal convection during solvent evaporation, as well as electronic traps formed during perovskite crystallization—are chief causes. Here, we report a molecular modification strategy that simultaneously eliminates pinholes in perovskite layers by controlling the dynamics of film formation and that passivates defects in perovskites by incorporating Br species, thereby preventing shorts and non-radiative recombination. The molecular modifier 1,3,5-tris (bromomethyl) benzene (TBB) also modulates the electronic structure of injection or transport materials to achieve improved charge injection and balanced charge transport. As a result, we demonstrate 20 mm × 20 mm green perovskite nanocrystal LEDs that achieve an external quantum efficiency (EQE) of over 16%, a record for large-area PeLEDs.

INTRODUCTION

Metal halide perovskite materials exhibit pure color emission, tunable band gap, flexibility, and solution processing,[1–8] making them promising candidates for low-cost and large-area light-emitting diodes (LEDs). The external quantum efficiency (EQE) of perovskite LEDs (PeLEDs) has increased in the past three years due to improved perovskite emitter quality and device architectures.[9–15] These achievements have, to date, been mainly limited to small-area (~4 mm^2) PeLEDs. Recently, advances have been seen in large-area (> 1 cm^2) PeLEDs[16–19]: Zhao et al. demonstrated a 12.1% EQE large-area PeLEDs with an emission peak at ~800 nm and an emission area of 30 mm × 30 mm. They achieved this by improving charge balance using a hole-transporting polymer with a shallower ionization potential.[16]

Looking across spectral ranges of interest from the blue to the near infrared (NIR), large-area PeLEDs, nevertheless, lag behind the corresponding small-area devices. Significant loss in performance arises when the emitting area of solution-processed films increases. Microscopic defects are dominant due to boundaries among perovskite domains[20] and non-uniform coating,[21,22] as well as non-radiative electronic traps.[23,24] Considerable efforts have been devoted to address these issues in small-area PeLEDs. Doping charge transport layers (CTLs)[25] or inserting interlayers

Context & Scale

Defects and electronic traps in perovskite films are chief causes that limit the performance of large-area perovskite light-emitting diodes (PeLEDs). Herein, we developed a molecular interface control strategy that eliminates pinholes in the large-area perovskite layers by controlling the dynamics of film formation while simultaneously passivating the defects in perovskites by incorporating Br species. The strategy thus prevents both shorts and non-radiative recombination, all the while providing improved charge injection or transport. These improvements enable a record-efficiency green perovskite nanocrystal LED with an external quantum efficiency (EQE) of 20.1%; in addition, we demonstrate a 20 mm × 20 mm large-area PeLED with a high EQE of over 16%. Our work contributes a notable advance to the community in the selection of interfacial layer materials, the scalable film deposition technique, an insight into underlying mechanisms, and performance.

between the CTL and emissive layer[9,26] have been investigated as a means to reduce interfacial recombination losses. Additives such as ligands and molecules have been adopted to passivate surface defects in perovskite nanocrystal (PeNC), and therefore, increase photoluminescence quantum yield (PLQY).[23,27] Surface treatments have been applied to deposit smooth and dense PeNC films to reduce the leakage current,[28,29] especially important in large-area PeLEDs. In light of the application of PeLEDs in next-generation display and solid-state lighting technologies, further development of efficient large-area PeLEDs is of interest.

We took the view that a judiciously selected interfacial layer between the PeNCs and injection layers would need to be designed such that it simultaneously (1) improved film morphology, enabling fabrication of a smooth, dense emissive layer (EML) in large-scale; (2) passivated the surface defects of PeNCs and suppressed quenching of PeNCs emission at the PeNC-hole transport layer (HTL) interface; and (3) improved hole injection, leading to enhancement in charge balance.

Herein, we report a molecular interface control strategy of incorporating 1,3,5-tris (bromomethyl) benzene (TBB) with an electron-accepting character, a halide-rich nature, and a small molecule structure between HTL and EML to simultaneously achieve pinhole-free smooth and dense large-area PeNC layers, improvement in surface passivation of PeNCs, as well as balanced charges, compared with the control device without TBB inserted. As a result, green PeNC LEDs with a large emitting area of 20 mm × 20 mm exhibit an EQE of 16.3%.

RESULTS AND DISCUSSION

Preparation of PeNC Films

Uniformity and full coverage of EMLs play significant roles in achieving high-performance large-area PeLEDs. In our study, we prepared 20mm × 20 mm large-area $FAPbBr_3$ PeNCs on poly(4-butylphenyl-diphenyl-amine) (poly-TPD) HTL and found pits in NC films. This we ascribe to thermal convection during solvent evaporation. Since $FAPbBr_3$ perovskite incorporates Br, an interfacial molecule modifier that possesses Br could potentially enable scalable fabrication of solution-processed $FAPbBr_3$ NC films: Increased particle-molecule interaction between the PeNCs and the TBB during film formation would improve large-area coverage.

We then applied a thin layer of TBB on poly-TPD, which is Br rich (Figure S1). Energy-dispersive X-ray (EDX) mapping images of the overlying TBB film show a homogeneous distribution of Br, indicating that the TBB molecules are uniformly deposited on the poly-TPD film (Figure S2). Field-emission scanning electron microscopy (FE-SEM) was performed to examine the influence of TBB on the surface morphology of PeNCs on HTL. As shown in Figure 1, a uniform and close-packed PeNC film was formed when the PeNC solution is spin casted on to the TBB-coated poly-TPD. This finding indicates that this thin TBB layer enables the large-area deposition of smoother and denser PeNC layers due to the strong Br–Br bonding and the improved surface quality for the underneath poly-TPD layer (Figures S3–S5 and Note S1).

Passivation of PeNC Films

We further investigated the effect of TBB on PeNC film quality. TBB also passivates $FAPbBr_3$ PeNCs and reduces the quenching of PeNC emission caused by the poly-TPD HTL. Our $FAPbBr_3$ PeNCs achieved high PLQYs of > 95% (in hexane) (Figure S6; Note S2). When the PeNCs are spin coated on poly-TPD-coated substrates, the

[1]Key Laboratory of Advanced Display and System Applications of Ministry of Education, Shanghai University, 149 Yanchang Road, Shanghai 200072, China

[2]Department of Electrical and Computer Engineering, University of Toronto, 35 St. George Street, Toronto, ON M5S 1A4, Canada

[3]Institute of Solar Energy Materials and Devices, College of Materials Science and Engineering, Sichuan University, 24 South Section 1, Yihuan Road, Chengdu 610065, China

[4]Department of Physics and Astronomy and Wright Center for Photovoltaics Innovation and Commercialization, The University of Toledo, Toledo, OH 43606, USA

[5]School of Physical Science and Technology, Shanghai Tech University, 393 Middle Huaxia Road, Pudong, Shanghai 201210, China

[6]These authors contributed equally

[7]Lead Contact

*Correspondence: yanfa.yan@utoledo.edu (Y.Y.), ted.sargent@utoronto.ca (E.H.S.), yangxy@shu.edu.cn (X.Y.)

https://doi.org/10.1016/j.joule.2020.07.002

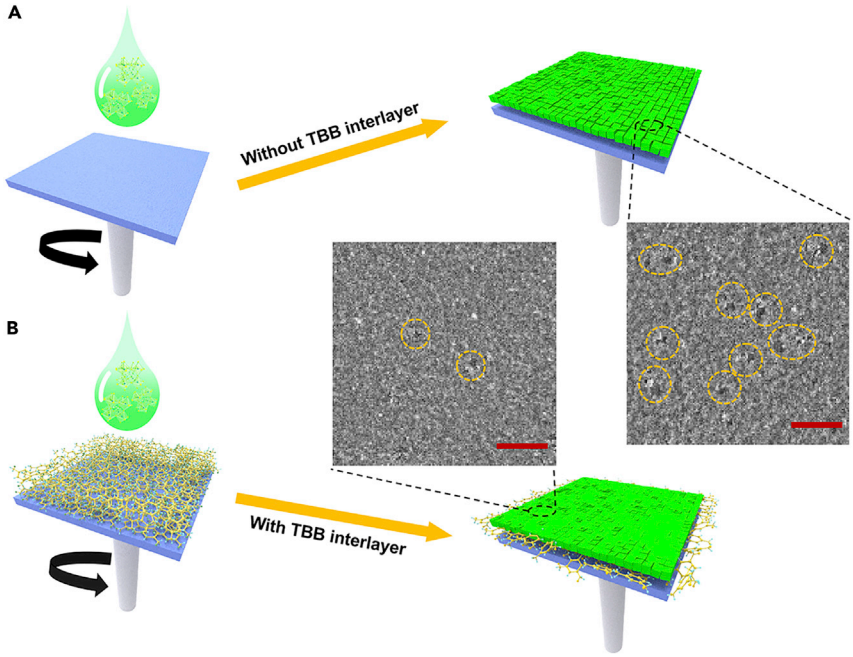

Figure 1. Molecular Interface Modifiers to Scale Perovskite NC Films
(A and B) Deposition of PeNC solutions on (A) poly-TPD and (B) poly-TPD modified by TBB. All scale bars are 500 nm.

PeNCs show much-reduced PLQYs and photoluminescence (PL) lifetime in the absence of TBB. We attribute this to charge transfer (CT) at the PeNC-poly-TPD interface,[26] resulting in quenching of the PeNC radiative emission (Figure S7; Table S1).

We also employed PL and time-resolved PL (TRPL) measurements to study the interaction between TBB and the surface of PeNCs (Figures 2A–2C). The PL intensity of PeNC films is enhanced with increased TBB atop the poly-TPD layer (Figures 2A and 2B). The PL emission peaks of the PeNCs deposited on TBB are blue shifted compared with those of the PeNCs without TBB. The average carrier lifetime (τ_{ave}) of PeNC films increases from 12 to 28 ns with increasing TBB concentration (Figure 2C; Table S2). Similar PL lifetime trends are exhibited in the case without poly-TPD in which CT from PeNCs to poly-TPD is excluded (Figure S8). These findings indicate that TBB molecules passivate the defects on PeNCs, leading to enhanced radiative emission efficiency of the PeNCs.[30–34]

We attribute the excellent passivation of TBB to the halide-rich environment that it provides to the PeNC surface.[35–38] X-ray photoelectron spectroscopy (XPS) analysis reveals that the Br species in TBB are incorporated on the surface of PeNCs. As shown in Figures 2D and S9, the binding energy peaks of Br3d at 68.7 eV ($Br3d_{5/2}$) and 69.8 eV ($Br3d_{3/2}$) for the PeNCs with TBB are shifted to higher positions compared with those of the PeNCs without TBB due to more electronegative Br^- in TBB molecules.[39] The processing method further augments the bonding between the Br^- of TBB and surfaces of PeNCs, allowing full leveraging of its passivation function. As shown in Figure S10, the τ_{ave} (26.6 ns) of the PeNCs fabricated using the new process exceeds that (17 ns) achieved using conventional processing (i.e., spin coating PeNC solution on a dry TBB film with post-annealing treatment).

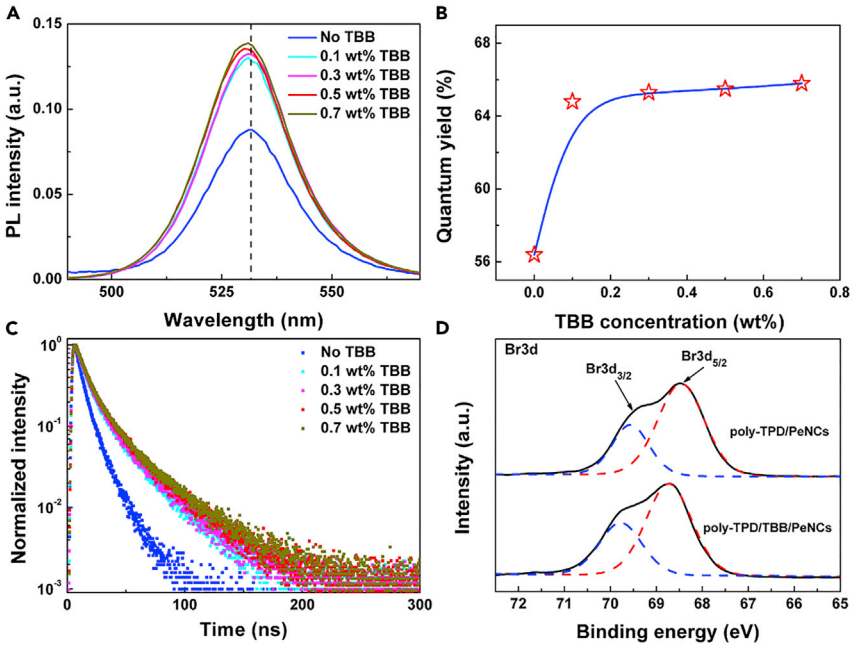

Figure 2. Passivation Effects of TBB on PeNC Films

(A–C) PL spectra (A), PLQYs (B), and PL decay curves (C) of PeNC films treated with different concentrations of TBB solutions on glass/poly-TPD substrates.

(D) XPS spectra (binding energy peaks for $Br3d_{5/2}$ and $Br3d_{3/2}$) of PeNCs on ITO/poly-TPD and ITO/poly-TPD/TBB (0.5 wt %) substrates.

Mechanism of Lowering the Highest Occupied Molecular Orbital Level Using TBB

Balance of charge injection and transport is crucial for efficient LEDs.[26] It is found that a relatively large offset (~ 0.6 eV) in the highest occupied molecular orbital (HOMO) levels occurs at the poly-TPD-PeNC interface. TBB with deep-lying electronic states is applied on top of poly-TPD with the goal of lowering the HOMO level via surface doping. Using ultraviolet photoemission spectroscopy (UPS), we analyzed the effect of TBB on the electronic structure of the poly-TPD surface in order to quantify the electronic properties of the materials. The HOMO of poly-TPD increases monotonically from −5.10 to −5.42 eV with increasing TBB concentration, indicating that the TBB molecule adjusts the HOMO level of poly-TPD (Figures 3A and S11; Table S3). We also find that TBB modifier works for a wide range of HTLs. The common hole transport materials widely used in nanocrystal-based LEDs, such as poly(9-vinylcarbazole) (PVK) and poly[9,9-dioctylfluorene-co-N-[4-(3-methylpropyl)]-diphenylamine] (TFB), were studied to observe that their HOMO levels are downshifted, suggesting a general strategy of adjusting HOMO levels (Figure S12; Table S4).

PL spectra show severe PL quenching of poly-TPD in the presence of the TBB layer (Figure 3B). The PL quenching is more dramatic when we further increase the TBB concentration. This indicates that efficient non-radiative CT occurs from poly-TPD to TBB. As shown in Figure 3C, TBB—in light of the electronegativity of bromine—possesses an electron-accepting character (deep lowest unoccupied molecular orbital [LUMO]) (Figure S13; Table S5), while poly-TPD has a strong electron-donating character, given its lone pair nitrogen atom on the triphenylamine unit that contributes to conjugation with the π-system and increases electron

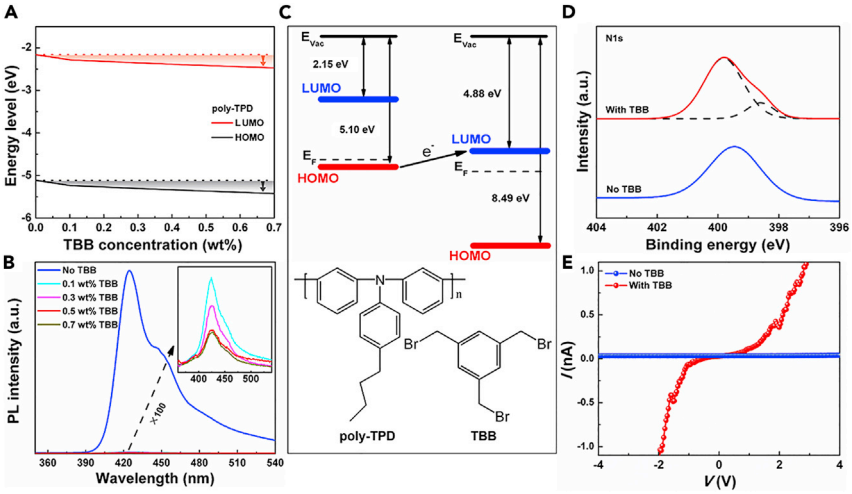

Figure 3. Effects of TBB on the Optical and Electrical Properties of Poly-TPD

(A and B) Electronic structure (A) and PL spectra (B) of poly-TPD films treated with different concentrations of TBB solution. Inset in (B): PL spectra of poly-TPD/TBB films when we increase the TBB concentration from 0.1 to 0.7 wt %.

(C) Schematic illustration of electron transfer from the HOMO of poly-TPD to the LUMO of TBB and the chemical structures for poly-TPD and TBB molecules.

(D) Binding energy of N1s in poly-TPD films without and with TBB (0.5 wt %) treatment.

(E) *I-V* characteristics of the corresponding poly-TPD films without and with TBB (0.5 wt %) treatment measured using C-AFM.

delocalization.[32] The relatively small energy offset of ~0.22 eV between the HOMO of poly-TPD and LUMO of TBB facilitates electron transfer from poly-TPD to TBB, introducing holes into poly-TPD, i.e., producing net p type doping. We also note that the close values for the LUMO of TBB and HOMO of HTLs are beneficial for p doping using TBB due to the reduced CT barrier.

XPS results (Figure 3D) reveal energy band bending from poly-TPD to the interface and the accumulation of electrons in TBB, confirming the p doping of poly-TPD via interfacial CT (Note S3). π-electron delocalization due to the CT process enables an enhancement in the electrical conductivity of poly-TPD surface, as revealed using conductive atomic force microscopy (c-AFM) (Figure 3E). A significant increase in current is observed when only a very small bias is applied to the indium tin oxide (ITO)/poly-TPD/TBB architecture, compared with the one without TBB.

Device Structure and Performance

We fabricated 20 mm × 20 mm large-area PeLEDs with and without a TBB interlayer. The device architecture (Figure 4A) and corresponding cross-sectional transmission electron microscope (TEM) image reveal a multi-layer structure consisting of ITO/poly (3,4-ethyllenedioxythiophene)-poly(styrenesulfonate) (PEDOT:PSS)/poly-TPD/TBB/$FAPbBr_3$ NCs/1,3,5-tris(1-phenyl-1H-benzimidazol-2-yl)benzene (TPBI)/lithium fluoride (LiF)/Al. Their corresponding schematic energy level diagram in Figure 4B shows that electrons are injected from the LiF/Al cathode and transported to the PeNC EML via the LUMO of TPBI. Hole injection is more challenging due to the high energy barrier (~ 0.6 eV) from the HOMO of poly-TPD to the valence band maximum (VBM) of PeNCs. Once we downshift the HOMO level by ~ 0.3 eV for poly-TPD using the TBB interlayer, the barrier is reduced and hole injection efficiency is improved. The surface electronic structure of poly-TPD film is modified by TBB molecules (Figure S14; Table S6), indicating no negative effects on hole injection from PEDOT:PSS to poly-TPD.

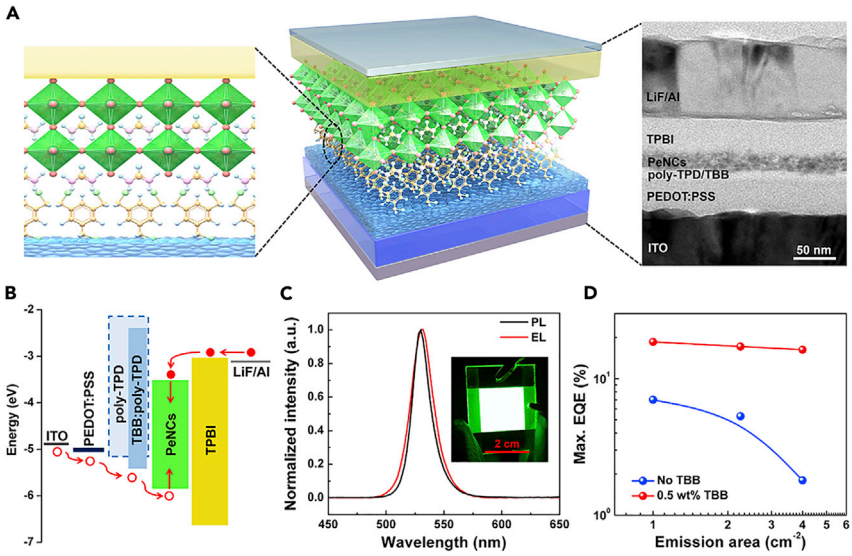

Figure 4. Device Structure and Analysis of Electrical Properties of PeLEDs

(A) Device architecture and cross-sectional TEM image of the multi-layer PeLEDs: ITO/PEDOT:PSS (40 nm)/TBB-modified poly-TPD (15 nm)/PeNCs (20 nm)/TPBI (40 nm)/LiF (1 nm)/Al (100 nm); the thickness of the TBB interlayer corresponding to a 0.5 wt % TBB concentration is ~2.6 nm (Figure S18).

(B) Energy band diagram for the resultant PeLED devices. The dash line in (B) represents the energy level of poly-TPD. The energy levels for PeNCs and TPBI are taken from Zhang et al.[40] and Cho et al., respectively.[41]

(C) Normalized PL and EL spectra of the PeNCs and a typical PeLED with TBB (0.5 wt %) interlayer at an applied voltage of 4 V. Inset: The photograph in (C) shows a large-area PeLED with the size of 20mm × 20 mm operating at 4.5 V.

(D) Dependence of maximum EQE on device emission area.

Figure 4C shows an electroluminescence (EL) spectrum of a resulting PeLED with the TBB-modified gradient HTL. Devices were measured in ambient conditions and without encapsulation. The spectrum shows an emission peak at ~531 nm and a full width at half maximum (FWHM) of 20 nm. The sharp emission peak corresponds to the Commission Internationale de 1′ Eclairage (CIE) color coordinates of (0.19, 0.73), indicating the high color purity (Figure S15), as desired in lighting and display applications. The EL emission wavelength is slightly broadened and red shifted by ~3 nm compared with the PL emission wavelength of PeNC solution, a fact we ascribe to the combination of finite dot-to-dot interaction in close-packed solid films and electric-field-induced Stark effect.[42–44]

The EQE for the device with TBB reaches 16.3% at active area of 20 mm × 20 mm (Figure S16; Table S7), while the efficiency for the devices without TBB decreases with increasing emitting area and the maximum EQE is reduced to 1.8% for the same emitting area (Figures 4D and S17; Table S8).

In order to clarify the effect of TBB on device operation, we carried out electrical characterization to compare with small-area (small emitting area of 2 mm × 2 mm) PeLEDs. We fabricated single-carrier devices to further assess the role of the TBB interlayer in promoting hole injection. As shown in Figure 5A, the current density for hole-only devices increases and approaches the efficacy of electron injection (Figure S19) when a TBB interlayer is deposited. It compares favorably with the case of hole-only devices without the TBB interlayer and produces improved charge balance in PeNC-based PeLEDs.

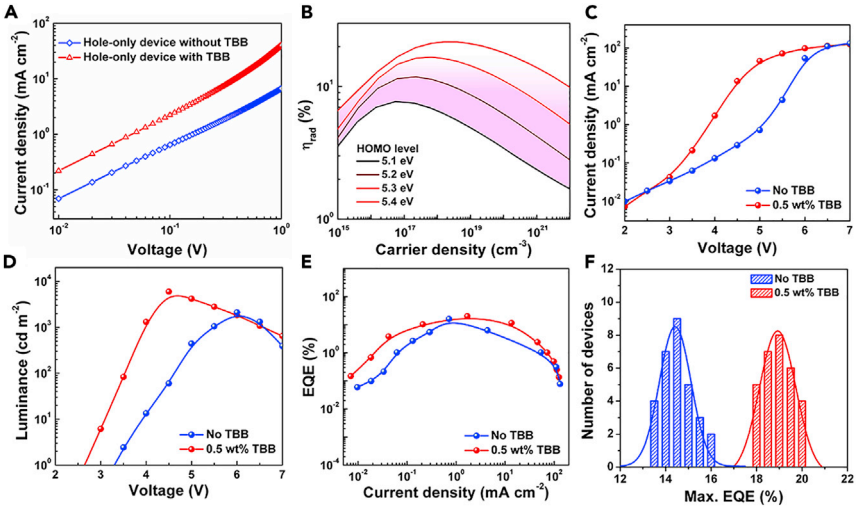

Figure 5. Comparison for EL Performance of PeLEDs without and with TBB

(A) *J-V* characteristics for the hole-only devices with the structures ITO/PEDOT:PSS/poly-TPD/PeNCs/MoO_x (8 nm)/Au (100 nm) and ITO/PEDOT:PSS/poly-TPD/TBB/PeNCs/MoO_3 (8 nm)/Au (100 nm). All the thicknesses not marked for other functional layers are the same with those in PeLEDs.

(B) η_{rad} at different carrier densities of HTLs with different HOMO levels.

(C–E) J-V (C), *L-V* (D), and *EQE-J* (E) curves of the resulting PeLEDs without and with 0.5 wt % TBB interlayer.

(F) Histogram of max. EQE of 30 devices with the same fabrication condition.

To explore the role of charge balance further, we also carried out optoelectronic device modeling to simulate the effect of shifting the HOMO level of the injecting layer on device performance (Figure S20). We varied the electron affinity of poly-TPD to simulate the changes in the HOMO level of poly-TPD (Table S9). We further extracted the internal quantum efficiency of the devices η_{rad}, which is the fraction of injected carriers that produce the emission of photons from PeNCs. The results (Figure 5B) show that, over the range of the injected carrier density employed in PeLEDs, devices with a deep HOMO level yield the highest efficiencies, and that this results from a more balanced charge distribution when the hole injection barrier is small.

We applied TBB to a range of hole injection/transport materials to check how widely applicable is the approach. Hole injection for each of these functional layers is significantly enhanced once TBB is deposited (Figures S21–S23; Table S10). The PeLED device structure of ITO/PEDOT:PSS/poly-TPD/TBB shows optimal performance due to efficient gradient hole injection.

The current density-voltage (*J-V*) characteristics of the PeLED (Figure 5C) show that the current density increases by orders of magnitude from 2 to 6 V as TBB is incorporated compared with the control device, indicating improved hole injection and balanced charge carrier transport. Figures 5D and 5E compare the *L-V* and *EQE-J* characteristics of the PeLEDs without and with TBB interlayer. The maximum luminance (5,980 cd m^{-2}) of the PeLED with TBB is higher than that of the PeLED without TBB (2,120 cd m^{-2}). The turn-on voltage of the PeLED with TBB is 2.6 V, below that of the PeLED without TBB (3.3 V). The maximum CE (77.2 cd A^{-1}) and EQE (20.1%) of the PeLED with the TBB interlayer approach the theoretical efficiency value of PeLEDs,[13] much higher than the efficiency values of the PeLED without TBB (max. CE: 61.4 cd A^{-1} and max. EQE: 16.0%) (Figures S24–S27; Table S11). Figure 5F

presents the histogram of the maximum EQE values for 30 devices with TBB and without TBB under the respective optimal conditions. The average maximum EQE values for these devices with and without TBB are 19.0% and 14.5%, respectively. Each device class shows low standard deviation (3.5% relative for PeLEDs with TBB & 5.6% relative for PeLEDs without TBB), demonstrating good reproducibility.

The instability of present-day PeLEDs remains an issue that must be overcome on the path to practical application. The PeLED that employed TBB (80% lifetime $T_{80} \sim$ ca. 2.9 h) exhibited an appreciable enhancement in operating lifetime compared with the PeLED without TBB (80% lifetime $T_{80} \sim$ ca. 1.8 h) (Figure S28), which is attributed to simultaneous improvements in film uniformity, passivation of PeNCs, and charge balance, as aforementioned. The device operating lifetime in this work is comparable with the longest lifetimes reported in PeLEDs at similar luminance.[12,45] The results suggest a promising strategy to improve both performance and stability. It can also be expected that further improvement in the stability of PeNC-based LEDs will be had by developing more stable PeNCs, doping suitable metal ions to stabilize perovskite lattices[46] and exchanging surface capping ligands to better passivate PeNCs.[47]

Conclusions

We demonstrate large-area (20 mm × 20 mm) PeLEDs that exhibit EQE of 16.3% enabled by the new multi-functional interlayer TBB due to enhancement in large-area film uniformity, passivation of PeNCs by improved Br bonding, and modulated charge injection/transport balance. As a result, we also achieve the highest EQE—reaching over 20%—reported in green PeNC LEDs. This work offers a route to the fabrication of scaled PeLEDs.

EXPERIMENTAL PROCEDURES

Resource Availability

Lead Contact

Further information and requests for resources and materials should be directed to and will be fulfilled by the lead contact, Xuyong Yang (yangxy@shu.edu.cn).

Materials Availability

This study did not generate new unique materials.

Data and Code Availability

The data presented in this work are available from the corresponding authors upon reasonable request.

Materials

$Pb(acetate)_2 \cdot 3H_2O$ (Sinopharm Chemical Reagent, AR, ≥99.5%), FA-acetate (Sigma-Aldrich, 99%), OAmBr (Xi'an P-OLED, 99.5%), Octane (Sinopharm Chemical Reagent, CP, ≥98%), Hexane (Sinopharm Chemical Reagent, AR, ≥97%), Ethyl acetate (Sinopharm Chemical Reagent, AR, ≥99.5%), DDAB (Sigma-Aldrich, 98%), and oleic acid (OA, Sigma-Aldrich, 90%). TBB (J&K Reagent, 98%). Toluene (Sinopharm Chemical Reagent, AR, ≥99.5%), Chlorobenzene (Sinopharm Chemical Reagent, AR, ≥99.5%), and PEDOT:PSS (Clevious PVP AI 4083) were purchased from Heraeus. PVK, TPBI and LiF were purchased from Luminescence. poly-TPD and TFB were purchased from American Dye Source (ADS). All materials were used as received.

Preparation of $FAPbBr_3$ NCs

$Pb(acetate)_2 \cdot 3H_2O$ (0.076 g, 0.2 mmol), FA-acetate (0.078 g, 0.75 mmol), OAmBr (0.21 g, 0.6 mmol), dried OA (2 mL, 6.3 mmol), and octane (8 mL) were loaded into a 25 mL beaker, and the reaction medium was subjected to tip-ultrasonication (SONOPULS HD 3100, BANDELIN) at a power of 35 W for 1 min.

For purification of $FAPbBr_3$ NCs, 30 mL of ethyl acetate was added into the crude solution and the mixture was centrifuged for 5 min at 7,500 rpm. The supernatant was discarded, the bottom precipitate was re-dispersed in 2 mL hexane, and the solution was then centrifuged for 1 min at 7,500 rpm. The precipitate was discarded, and 6 mL ethyl acetate was added into the solution. The precipitate was collected separately after centrifugation and finally dispersed in 2 mL hexane at a concentration of 6 mg/mL.

Treatment of $FAPbBr_3$ NCs for PeLED fabrication: 2 mL of the purified $FAPbBr_3$ NCs, 50 μL of OA was added under stirring, then 100 μL DDAB toluene solution (0.05 M) was added. 4 mL ethyl acetate was added into the solution. The precipitate was collected after centrifugation and finally dispersed in 2 mL hexane.

Device Fabrication

The patterned ITO glass substrates were sequentially sonicated with detergent, deionized water, acetone, and isopropyl alcohol for 15 min each. After being dried using nitrogen, the substrates were transferred into oxygen plasma and treated for 15 min. PEDOT:PSS was spin coated onto the pre-cleaned and oxygen plasma-treated ITO substrates at a speed of 4,000 rpm for 40 s and then baked at 150°C for 10 min in air. The substrates were then transferred into a nitrogen glove box (H_2O and $O_2 \leq$ 0.1ppm), and a solution of poly-TPD (dissolved in chlorobenzene with a concentration of 8 mg/ml) was spin cast onto the PEDOT:PSS film at a speed of 4,000 rpm for 1 min and then baked at 150°C for 20 min. The wet TBB layer is obtained by spin coating TBB solution in toluene on top of poly-TPD film at a speed of 5,000 rpm for 1 min without post-annealing. For $FAPbBr_3$ NC layer deposition, the $FAPbBr_3$ NC solution was spin coated at a speed of 1,500 rpm for 1 min. The samples were then transferred into a vacuum chamber. The 40 nm TPBI, 1 nm LiF, and 100 nm Al layers were sequentially deposited by thermal evaporation in a vacuum thermal evaporation clamber at a pressure $<4 \times 10^{-4}$ Pa.

Characterization

UPS and XPS were acquired using a Thermo Scientific Escalab 250Xi. UPS measurements were obtained using a He (I) photo line (21.22 eV) from a He discharge lamp. AFM and C-AFM measurements were performed using Bruker dimension icon microscope. XRD patterns were obtained using a Bruker D8 advance diffractometer with Cu Kα radiation as the X-ray source. FE-SEM measurements were conducted using a JEOL JSM-7500F microscope. Absorption spectra were measured using a PerkinElmer Lambda 950 UV-vis-NIR spectrometer. PL, PLQYs, and TRPL spectra were obtained using an Edinburgh FLS920 PL spectrometer. Thickness measurements for TBB layers were carried out using W-VASE with AutoRetarderTM ellipsometer. The EL characteristics of the PeLEDs were collected using a system comprised of PR-670 spectra scan spectroradiometer coupled with a Keithley 2400 source meter. The EL characteristics for devices with TBB at the emission area of 2 mm × 2 mm were verified using a fiber integration sphere (FOIS-1) coupled with a QE Pro650 spectrometer and the Keithley 2400 source meter for current density-voltage characterization. The LED was tested on top of the integrating sphere, which has been accurately calibrated by a commercially standard LED. The device lifetime tests of PeLEDs were performed on a ZJZCL-1 OLED aging lifespan test instrument.

Optoelectronic Simulations

Calculations were carried out using the SCAPS 3. 0.07 1D modeling suite.[6,48] Ohmic boundary conditions were implemented on each electrode. Experimental band gaps, band alignments, mobilities, and active layer thicknesses were used (Supplemental Information, SCAPS parameters). HOMO levels of poly-TPD from −5.1 to −5.4 eV were chosen based on the measured energy levels in Table S3.

SUPPLEMENTAL INFORMATION

Supplemental Information can be found online at https://doi.org/10.1016/j.joule.2020.07.002.

ACKNOWLEDGMENTS

The authors acknowledge the financial support from the National Natural Science Foundation of China (nos. 51675322, 61605109, and 61735004), the National Key Research and Development Program of China (no. 2016YFB0401702), the Shanghai Science and Technology Committee (no. 19010500600), and the Program for Professor of Special Appointment (Eastern Scholar) at Shanghai Institutions of Higher Learning. D.Z. also thanks the financial support by the Science and Technology Program of Sichuan Province (no. 2020JDJQ0030) and the Fundamental Research Funds for the Central Universities (no. YJ201955). The authors also thank Aidan Grenville at University of Toronto for fruitful discussions and generous help.

AUTHOR CONTRIBUTIONS

X.Y. and E.H.S. proposed the research directions and guided the project. H.W., J.Z., L.K., and Y. S. fabricated and characterized the PeLED devices. X.G. and O.V. carried out optoelectronic simulations. H.W., Y.-B.Z., D.Z., X.G., S.W., B.W., R.Q.-B., O.V., Z.N., Y.Y., E.H.S., and X.Y analyzed and discussed the experimental results. H.W., X.G., D.Z., and Y.-B.Z. provided equal contributions to this study. All authors contributed to the manuscript.

DECLARATION OF INTERESTS

The authors declare no competing interests.

Received: February 14, 2020
Revised: June 1, 2020
Accepted: June 30, 2020
Published: July 29, 2020

REFERENCES

1. Tan, Z.K., Moghaddam, R.S., Lai, M.L., Docampo, P., Higler, R., Deschler, F., Price, M., Sadhanala, A., Pazos, L.M., Credgington, D., et al. (2014). Bright light-emitting diodes based on organometal halide perovskite. Nat. Nanotechnol. *9*, 687–692.

2. Xiao, Z., Kerner, R.A., Zhao, L., Tran, N.L., Lee, K.M., Koh, T., Scholes, G.D., and Rand, B.P. (2017). Efficient perovskite light-emitting diodes featuring nanometre-sized crystallites. Nat. Photon. *11*, 108–115.

3. Stranks, S.D., and Snaith, H.J. (2015). Metal-halide perovskites for photovoltaic and light-emitting devices. Nat. Nanotechnol. *10*, 391–402.

4. Song, J., Li, J., Li, X., Xu, L., Dong, Y., and Zeng, H. (2015). Quantum dot light-emitting diodes based on inorganic perovskite cesium lead halides ($CsPbX_3$). Adv. Mater. *27*, 7162–7167.

5. Shang, Y., Liao, Y., Wei, Q., Wang, Z., Xiang, B., Ke, Y., Liu, W., and Ning, Z. (2019). Highly stable hybrid perovskite light-emitting diodes based on Dion-Jacobson structure. Sci. Adv. *5*, eaaw8072.

6. Gong, X., Yang, Z., Walters, G., Comin, R., Ning, Z., Beauregard, E., Adinolfi, V., Voznyy, O., and Sargent, E.H. (2016). Highly efficient quantum dot near-infrared light-emitting diodes. Nat. Photon. *10*, 253–257.

7. Yin, W.J., Shi, T., and Yan, Y. (2014). Unique properties of halide perovskites as possible origins of the superior solar cell performance. Adv. Mater. Weinheim *26*, 4653–4658.

8. Chen, H., Lin, J., Kang, J., Kong, Q., Lu, D., Kang, J., Lai, M., Quan, L.N., Lin, Z., Jin, J., et al. (2020). Structural and spectral dynamics of single-crystalline Ruddlesden-Popper phase halide perovskite blue light-emitting diodes. Sci. Adv. *6*, eaay4045.

9. Lin, K., Xing, J., Quan, L.N., de Arquer, F.P.G., Gong, X., Lu, J., Xie, L., Zhao, W., Zhang, D., Yan, C., et al. (2018). Perovskite light-emitting diodes with external quantum efficiency exceeding 20 per cent. Nature *562*, 245–248.

10. Cao, Y., Wang, N., Tian, H., Guo, J., Wei, Y., Chen, H., Miao, Y., Zou, W., Pan, K., He, Y., et al. (2018). Perovskite light-emitting diodes based on spontaneously formed submicrometre-scale structures. Nature *562*, 249–253.

11. Liu, Y., Cui, J., Du, K., Tian, H., He, Z., Zhou, Q., Yang, Z., Deng, Y., Chen, D., Zuo, X., et al. (2019). Efficient blue light-emitting diodes based on quantum-confined bromide perovskite nanostructures. Nat. Photon. *13*, 760–764.

12. Chiba, T., Hayashi, Y., Ebe, H., Hoshi, K., Sato, J., Sato, S., Pu, Y., Ohisa, S., and Kido, J. (2018). Anion-exchange red perovskite quantum dots with ammonium iodine salts for highly efficient light-emitting devices. Nat. Photon. *12*, 681–687.

13. Zhao, B., Bai, S., Kim, V., Lamboll, R., Shivanna, R., Auras, F., Richter, J.M., Yang, L., Dai, L., Alsari, M., et al. (2018). High-efficiency perovskite–polymer bulk heterostructure light-emitting diodes. Nat. Photon. *12*, 783–789.

14. Wang, N., Cheng, L., Ge, R., Zhang, S., Miao, Y., Zou, W., Yi, C., Sun, Y., Cao, Y., Yang, R., et al. (2016). Perovskite light-emitting diodes based on solution-processed self-organized multiple quantum wells. Nat. Photon. *10*, 699–704.

15. Wang, H., Zhang, X., Wu, Q., Cao, F., Yang, D., Shang, Y., Ning, Z., Zhang, W., Zheng, W., Yan, Y., et al. (2019). Trifluoroacetate induced small-grained $CsPbBr_3$ perovskite films result in efficient and stable light-emitting devices. Nat. Commun. *10*, 665.

16. Zhao, X., and Tan, Z. (2020). Large-area near-infrared perovskite light-emitting diodes. Nat. Photon. *14*, 215–218.

17. Kim, D.B., Lee, S., Jang, C.H., Park, J.H., Lee, A., and Song, M.H. (2020). Uniform and large-area cesium-based quasi-2D perovskite light-emitting diodes using hot-casting method. Adv. Mater. Interfaces *7*, 1902158.

18. Lau, Y.S., Lan, Z., Li, N., and Zhu, F. (2020). Large-area cesium lead bromide perovskite light-emitting diodes realized by incorporating a hybrid additive. ACS Appl. Electron. Mater. *2*, 1113–1121.

19. Prakasam, V., Tordera, D., Di Giacomo, F., Abbel, R., Langen, A., Gelinck, G., and Bolink, H.J. (2019). Large area perovskite light-emitting diodes by gas-assisted crystallization. J. Mater. Chem. C *7*, 3795–3801.

20. Li, Z., Klein, T.R., Kim, D.H., Yang, M., Berry, J.J., van Hest, M.F.A.M., and Zhu, K. (2018). Scalable fabrication of perovskite solar cells. Nat. Rev. Mater. *3*, 1807.

21. Wu, Y., Yang, X., Chen, W., Yue, Y., Cai, M., Xie, F., Bi, E., Islam, A., and Han, L. (2016). Perovskite solar cells with 18.21% efficiency and area over 1 cm^2 fabricated by heterojunction engineering. Nat. Energy *1*, 1–7.

22. Ye, F., Tang, W., Xie, F., Yin, M., He, J., Wang, Y., Chen, H., Qiang, Y., Yang, X., and Han, L. (2017). Low-temperature soft-cover deposition of uniform large-scale perovskite films for high-performance solar cells. Adv. Mater. *29*, 1701440.

23. Song, J., Fang, T., Li, J., Xu, L., Zhang, F., Han, B., et al. (2018). Organic–inorganic hybrid passivation enables perovskite QLEDs with an EQE of 16.48%. Adv. Mater. *30*, e1805409.

24. Xing, J., Zhao, Y., Askerka, M., Quan, L.N., Gong, X., Zhao, W., Zhao, J., Tan, H., Long, G., Gao, L., et al. (2018). Color-stable highly luminescent sky-blue perovskite light-emitting diodes. Nat. Commun. *9*, 3541.

25. Kim, Y.H., Cho, H., Heo, J.H., Kim, T.S., Myoung, N., Lee, C.L., Im, S.H., and Lee, T.W. (2015). Multicolored organic/inorganic hybrid perovskite light-emitting diodes. Adv. Mater. *27*, 1248–1254.

26. Zhang, X., Lin, H., Huang, H., Reckmeier, C., Zhang, Y., Choy, W.C., and Rogach, A.L. (2016). Enhancing the brightness of cesium lead halide perovskite nanocrystal based green light-emitting devices through the interface engineering with perfluorinated ionomer. Nano Lett. *16*, 1415–1420.

27. Ban, M., Zou, Y., Rivett, J.P.H., Yang, Y., Thomas, T.H., Tan, Y., Song, T., Gao, X., Credgington, D., Deschler, F., et al. (2018). Solution-processed perovskite light emitting diodes with efficiency exceeding 15% through additive-controlled nanostructure tailoring. Nat. Commun. *9*, 3892.

28. Li, J., Xu, L., Wang, T., Song, J., Chen, J., Xue, J., Dong, Y., Cai, B., Shan, Q., Han, B., et al. (2017). 50-Fold EQE improvement up to 6.27% of solution-processed all-inorganic perovskite $CsPbBr_3$ QLEDs via surface ligand density control. Adv. Mater. *29*, 1603885.

29. Coe, S., Woo, W.K., Bawendi, M., and Bulović, V. (2002). Electroluminescence from single monolayers of nanocrystals in molecular organic devices. Nature *420*, 800–803.

30. Yantara, N., Bhaumik, S., Yan, F., Sabba, D., Dewi, H.A., Mathews, N., Boix, P.P., Demir, H.V., and Mhaisalkar, S. (2015). Inorganic halide perovskites for efficient light-emitting diodes. J. Phys. Chem. Lett. *6*, 4360–4364.

31. Lee, S., Park, J.H., Lee, B.R., Jung, E.D., Yu, J.C., Di Nuzzo, D., Friend, R.H., and Song, M.H. (2017). Amine-based passivating materials for enhanced optical properties and performance of organic-inorganic perovskites in light-emitting diodes. J. Phys. Chem. Lett. *8*, 1784–1792.

32. Wang, J., Liu, K., Ma, L., and Zhan, X. (2016). Triarylamine: versatile platform for organic, dye-sensitized, and perovskite solar cells. Chem. Rev. *116*, 14675–14725.

33. Shao, Y., Xiao, Z., Bi, C., Yuan, Y., and Huang, J. (2014). Origin and elimination of photocurrent hysteresis by fullerene passivation in $CH_3NH_3PbI_3$ planar heterojunction solar cells. Nat. Commun. *5*, 5784.

34. deQuilettes, D.W., Vorpahl, S.M., Stranks, S.D., Nagaoka, H., Eperon, G.E., Ziffer, M.E., Snaith, H.J., and Ginger, D.S. (2015). Solar cells. Impact of microstructure on local carrier lifetime in perovskite solar cells. Science *348*, 683–686.

35. Liu, P., Chen, W., Wang, W., Xu, B., Wu, D., Hao, J., Cao, W., Fang, F., Li, Y., Zeng, Y., et al. (2017). Halide-rich synthesized cesium lead bromide perovskite nanocrystals for light-emitting diodes with improved performance. Chem. Mater. *29*, 5168–5173.

36. Zhang, J., Yang, Y., Deng, H., Farooq, U., Yang, X., Khan, J., Tang, J., and Song, H. (2017). High quantum yield blue emission from lead-free inorganic antimony halide perovskite colloidal quantum dots. ACS Nano *11*, 9294–9302.

37. Zheng, X., Chen, B., Dai, J., Fang, Y., Bai, Y., Lin, Y., Wei, H., Zeng, X., and Huang, J. (2017). Defect passivation in hybrid perovskite solar cells using quaternary ammonium halide anions and cations. Nat. Energy *2*, 17102.

38. Li, F., Lin, F., Huang, Y., Cai, Z., Qiu, L., Zhu, Y., Jiang, Y., Wang, Y., and Chen, X. (2019). Bromobenzene aliphatic nucleophilic substitution guided controllable and reproducible synthesis of high quality cesium lead bromide perovskite nanocrystals. Inorg. Chem. Front. *6*, 3577–3582.

39. Naphade, R., Nagane, S., Shanker, G.S., Fernandes, R., Kothari, D., Zhou, Y., Padture, N.P., and Ogale, S. (2016). Hybrid perovskite quantum nanostructures synthesized by electrospray antisolvent-solvent extraction and intercalation. ACS Appl. Mater. Interfaces *8*, 854–861.

40. Zhang, X., Liu, H., Wang, W., Zhang, J., Xu, B., Karen, K., Zheng, Y., Liu, S., Chen, S., Wang, K., and Sun, X.W. (2017). Hybrid perovskite light-emitting diodes based on perovskite nanocrystals with organic-inorganic mixed cations. Adv. Mater. *29*, 1606405.

41. Cho, H., Jeong, S.H., Park, M.H., Kim, Y.H., Wolf, C., Lee, C.L., Heo, J.H., Sadhanala, A., Myoung, N., Yoo, S., et al. (2015). Overcoming the electroluminescence efficiency limitations of perovskite light-emitting diodes. Science *350*, 1222–1225.

42. Wood, V., Panzer, M.J., Caruge, J.M., Halpert, J.E., Bawendi, M.G., and Bulović, V. (2010). Air-stable operation of transparent, colloidal quantum dot based LEDs with a unipolar device architecture. Nano Lett. *10*, 24–29.

43. Sun, Q., Wang, Y.A., Li, L.S., Wang, D., Zhu, T., Xu, J., Yang, C., and Li, Y. (2007). Bright, multicoloured light-emitting diodes based on quantum dots. Nat. Photon. *1*, 717–722.

44. Zhao, J., Bardecker, J.A., Munro, A.M., Liu, M.S., Niu, Y., Ding, I.K., Luo, J., Chen, B., Jen, A.K., and Ginger, D.S. (2006). Efficient CdSe/CdS quantum dot light-emitting diodes using a thermally polymerized hole transport layer. Nano Lett. *6*, 463–467.

45. Zhang, S., Yi, C., Wang, N., Sun, Y., Zou, W., Wei, Y., Cao, Y., Miao, Y., Li, R., Yin, Y., et al. (2017). Efficient red perovskite light-emitting diodes based on solution-processed multiple quantum wells. Adv. Mater. *29*, 1606600.

46. Zou, S., Liu, Y., Li, J., Liu, C., Feng, R., Jiang, F., Li, Y., Song, J., Zeng, H., Hong, M., and Chen, X. (2017). Stabilizing cesium lead halide perovskite lattice through Mn(II) substitution for air-stable light-emitting diodes. J. Am. Chem. Soc. *139*, 11443–11450.

47. Pan, J., Shang, Y., Yin, J., De Bastiani, M., Peng, W., Dursun, I., Sinatra, L., El-Zohry, A.M., Hedhili, M.N., Emwas, A.H., et al. (2018). Bidentate ligand-passivated $CsPbI_3$ perovskite nanocrystals for stable near-unity photoluminescence quantum yield and efficient red light-emitting diodes. J. Am. Chem. Soc. *140*, 562–565.

48. Burgelman, M., Decock, K., Khelifi, S., and Abass, A. (2013). Advanced electrical simulation of thin film solar cells. Thin Solid Films *535*, 296–301.